



# 增材制造的含硼 Ti-6Al-4V 钛合金的组织与性能研究

李长富<sup>1\*</sup>, 任皓显<sup>1</sup>, 步佳顾<sup>1</sup>, 王向明<sup>2</sup>, 杨光<sup>1</sup>

<sup>1</sup> 沈阳航空航天大学航空制造工艺数字化国防重点学科实验室, 辽宁 沈阳 110136;

<sup>2</sup> 中航工业沈阳飞机设计研究所, 辽宁 沈阳 110035

**摘要** 第二相相对增材制造钛合金材料的组织与性能有显著影响。将不同质量分数的 B 粉与 Ti-6Al-4V 粉末混合, 在激光沉积制造(LDM)工艺下制备出块状样品, 结合样品的室温拉伸性能, 对第二相在显微组织形成、基体形变过程中的强化机制进行了讨论。研究结果表明, 在 LDM 过程中, B 与 Ti-6Al-4V 合金中的 Ti 发生原位反应, 生成针状 TiB 第二相, 并均匀分布于基体中。随合金中 TiB 含量的增加, 原始  $\beta$  柱状晶尺寸逐渐减小, 晶内片层状  $\alpha$  相逐渐粗化, 合金的室温拉伸强度和塑性均获得提高。TiB 与基体  $\alpha$  相间具有严格晶体学位相关系, 在阻碍基体应变过程中, 针状 TiB 易沿直径方向断裂, 断裂处在随后的形变过程中形成孔洞。最佳强化效果出现在含有 B 粉质量分数为 0.1% 的样品中, 原因在于当合金中 B 粉质量分数过大时, 会出现过多的针状 TiB 断裂, 此时连续孔洞转变为微裂纹, 导致材料塑性下降。

**关键词** 激光技术; 激光增材制造; 钛合金; 原位反应; 显微结构; 力学性能

中图分类号 O436

文献标志码 A

doi: 10.3788/CJL202148.1802014

## 1 引言

钛合金具有比强度高、抗腐蚀性佳、高温下性能稳定的优点, 故被广泛应用航空、航天、国防、航海、电子、交通运输、医疗等领域<sup>[1-2]</sup>。随着钛合金使用要求及服役条件的提高, 其缺点也逐渐显现出来, 如耐热性不足、晶界易软化、耐磨性差, 故迫切需要通过成分调控、工艺优化、第二相强化等措施来强化钛合金。

第二相强化是钛合金强化最直接有效的方法<sup>[3-4]</sup>。钛合金第二相生成方法包括伴随快速凝固的半固态加工法<sup>[5-6]</sup>、塑性变形和热处理引起的再结晶法<sup>[7-9]</sup>、不同粒度粉末混合物的固化方法<sup>[10]</sup>和粉末烧结过程中的再结晶法<sup>[11]</sup>等。通过在钛合金中引入第二相的方式, 钛合金的强度和塑性均得到了一定的提升, 但第二相粒子团聚生长、单粒子尺寸变化、孔洞增多和基体显微组织粗化等问题仍需解决<sup>[12-15]</sup>。

增材制造技术是以金属粉末为原料, 利用高能束逐点熔化原料来逐层制造零件的, 故利用增材制造技术对第二相颗粒的分布及尺寸进行控制具有高度可行性。

利用增材制造技术可实现具有 Ti-SiC 网络结构的复合材料的制备。引入增强相网络( $Ti_5Si_3 + Ti_2C$ )可使制备的复合材料的屈服强度明显提高, 进而在 TiB/TC4 复合材料<sup>[16-17]</sup>中进一步引入  $Ti_5Si_3$  纳米强化相, 复合材料的拉伸强度可提高到 15%, 延伸率可保持在 5% 以上。

在利用激光沉积制造(LDM)技术制备的钛合金中, TiB 晶须使得材料的硬度比普通合金高 14.4%<sup>[18-19]</sup>。通过对高性能钢铁材料、高熵合金和大块非晶合金等先进金属材料<sup>[20-21]</sup>中的第二相强化机理的研究发现, 控制第二相的尺寸、体积比和形貌将大大提高这些材料的综合力学性能。

在现有文献中, B 通常以硼化物( $TiB_2$ 、 $TiB$  或  $B_4C$ )的形式被添加到粉末原料中。而纯 Ti 和 B

收稿日期: 2021-04-06; 修回日期: 2021-04-27; 录用日期: 2021-05-06

基金项目: 国家自然科学基金(51975387)、国家重点研发计划(2018YFB1105805)、航空科学基金(20184254003)

通信作者: \*20140029@sau.edu.cn

之间存在着极强的放热反应,该反应可以影响熔池凝固,第二相粒子的生成、分散程度和尺度等,进而最终会影响基体组织和材料的力学性能。目前,有关将纯B加入粉末原料制备第二相强化钛合金的报道较少。因此,本文采用LDM方法制备了TC4钛合金样品,通过在样品粉末中添加不同含量(质量分数,下同)纯B的方式来控制生成的第二相的总体含量,研究生成的第二相对合金组织及性能的影响,并对第二相的强化机制进行了探讨。

## 2 实验

采用沈阳航空航天大学的LDM-800激光增材制造系统进行实验样块的制备,激光增材制造系统包括:额定功率为6kW的光纤激光器、三坐标运动执行系统、三料仓同轴送粉器、氧含量测试仪及控制系统。

选用锻造退火态Ti-6Al-4V钛合金作为沉积基材,采用等离子旋转电极法制备Ti-6Al-4V粉末,粉末粒径的范围为45~180μm,粉末化学成分见表1。实验中使用的高纯B粉的粉末粒度范围为5~20μm。利用机械混合法将Ti-6Al-4V粉末与B粉混合,共制备了5组混合粉末。5组混合粉末的质量均为100g,其中B粉的含量分别为0.00%、0.05%、0.10%、0.20%和0.50%。

在沉积实验前,对Ti-6Al-4V粉末进行干燥处理,用砂轮和旋转锉打磨基材,并用乙醇擦拭清洗,去掉表面油污和氧化层。沉积实验的工艺参数为:

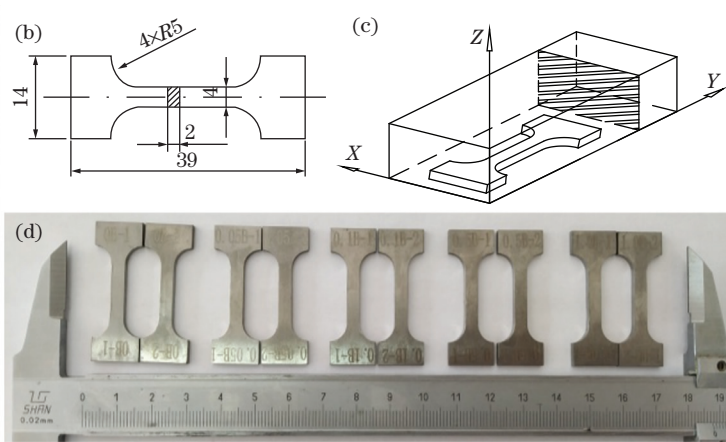


图1 采用LDM技术制备的Ti-6Al-4V沉积块及取样位置。(a)样品沉积态典型宏观形貌;(b)板状拉伸样品尺寸;(c)板状拉伸品取样位置及显微结构观察面(阴影面);(d)加工后的5组板状拉伸试样

Fig. 1 Ti-6Al-4V deposited block prepared by LDM technology and sampling position. (a) Typical macromorphology of the sample at deposited state; (b) size of plate tensile sample; (c) sampling position of plate tensile sample and the observation plane of the microstructure (shaded surface); (d) 5 groups of plate tensile samples after machining

激光功率为1.5kW,扫描速率为8mm/s,扫描间距为2mm,层厚为0.5mm。实验后获得的沉积在X、Y、Z方向的尺寸分别为25,50,8mm。图1展示了采用LDM工艺制备的Ti-6Al-4V沉积块及取样位置。图1(a)展示了B粉含量为0.05%的样块。沿平行基板平面(X-Y面)切取并制备的板状拉伸样品尺寸如图1(b)所示,其中R为半径。取样位置距离基板平面5mm以上,相对位置如图1(c)所示,显微结构的观察面如图1(c)中阴影面所示。从每个金属样块中取两支拉伸样品,制备好的五组板状拉伸样品如图1(d)所示。

对金相试样进行镶嵌、预磨和抛光操作后,再对其进行腐蚀操作,腐蚀液为HF-HNO<sub>3</sub>-H<sub>2</sub>O,三种不同液体的体积比为1:6:7。利用光学金相显微镜(OM)及扫描电子显微镜(SEM)对组织结构进行观察。利用Image-Pro Plus 6.0软件进行定量相分析,包括片层状α相的尺寸及长宽比。在电子万能试验机中进行室温拉伸性能测试。在X射线衍射(XRD)仪中进行XRD相分析(Cu K $\alpha$ 靶,衍射仪波长为 $1.5418 \times 10^{-10}$ m)。利用透射电子显微镜(TEM)进行微区组织观察及相鉴定,TEM的工作电压为200kV。

表1 Ti-6Al-4V钛合金粉末化学成分  
Table 1 Chemical compositions of Ti-6Al-4V titanium alloy powder

Element	Al	V	Fe	C	O	Ti
Mass fraction /%	6.37	4.09	$\leq 0.30$	$\leq 0.05$	$\leq 0.20$	Bal.



### 3 结果与分析

#### 3.1 相组成

图 2 为 LDM 制备的不同 B 含量的 Ti-6Al-4V 合金的 XRD 谱。曲线包含的衍射峰以  $\alpha$  相和  $\beta$  相衍射峰为主, 随着 B 含量增加, 第二相 TiB 衍射峰逐渐明显。当 B 元素含量为 0 时, 谱线中均为  $\alpha$  相或  $\beta$  相衍射峰。在增材制造沉积态中, Ti-6Al-4V 合金中  $\alpha$  相通常以针状或片状形式存在, 具体形式与熔池冷却速度有关<sup>[22-24]</sup>。

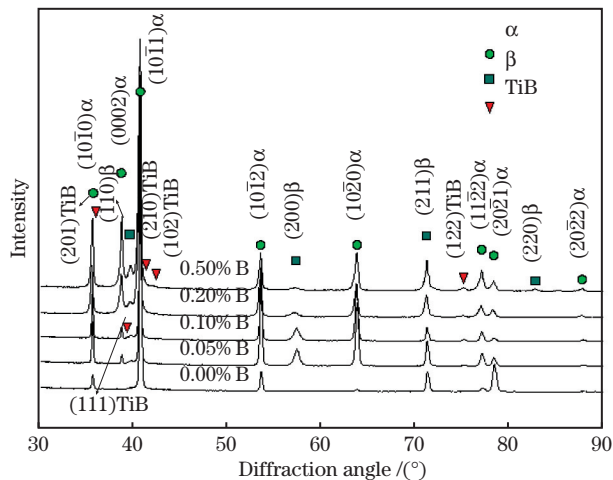


图 2 LDM 工艺制备的不同 B 含量的 Ti-6Al-4V 合金的 XRD 谱

Fig. 2 XRD spectra of Ti-6Al-4V alloys with different B contents prepared by LDM process

随着合金中 B 含量的增加,  $\alpha/\beta$  相衍射峰的比例发生变化, 但均以  $\alpha$  相衍射峰为主。其中, (0002) $\alpha$  峰相对强度随着 B 含量的增加明显增强, 主峰 (10 $\bar{1}$ 0) $\alpha$  以及 (10 $\bar{1}$ 2) $\alpha$  等相对强度变化明显。 $\beta$  相各衍射峰的强度也随 B 含量的增加在改变。增材制造的钛合金组织通常包含织构, 衍射峰相对强度的变化, 表明织构强度和类型在改变<sup>[25-28]</sup>。已有研究表明, B 添加对增材制造的钛合金的组织影响明显<sup>[29-30]</sup>, 其内在影响机制有待进一步研究。

当合金中 B 的含量增加至 0.10% 以上时, 谱线中的 TiB 衍射峰逐渐清晰, 说明在各个合金中其体积比在增大。其中, (122)TiB 衍射峰强度变化最为明显。XRD 结果表明, 纯 B 在 LDM 工艺条件下与合金中的 Ti 发生反应, 原位生成了硼化物第二相。

#### 3.2 组织形貌

增材制造的 Ti-6Al-4V 合金中通常包含原始  $\beta$  柱状晶, 柱状晶内部由片层状  $\alpha$  相或针状  $\alpha'$  相构成, 形成网篮组织、魏氏组织或马氏体组织<sup>[22, 31-32]</sup>, 柱状晶与  $\alpha$

相的尺寸由熔池温度梯度和固/液界面温度决定<sup>[33-34]</sup>。

图 3 为 LDM 技术制备的不同 B 含量的 Ti-6Al-4V 合金的显微结构形貌。在图 3(a)中, 未添加 B 元素的组织由原始  $\beta$  柱状晶构成, 柱状晶直径的范围为 600~800  $\mu\text{m}$ , 柱状晶长轴基本沿激光束入射方向生长。在 SEM 下, 可见原始  $\beta$  柱状晶内部全部由片层状  $\alpha$  相组成, 如图 3(b)所示, 利用 Image-Pro Plus 6.0 软件对图中片层状  $\alpha$  相尺寸进行定量分析后, 得出片层状  $\alpha$  相的平均宽度不足 1  $\mu\text{m}$ , 长度范围为 10~20  $\mu\text{m}$ , 长宽比约为 22。

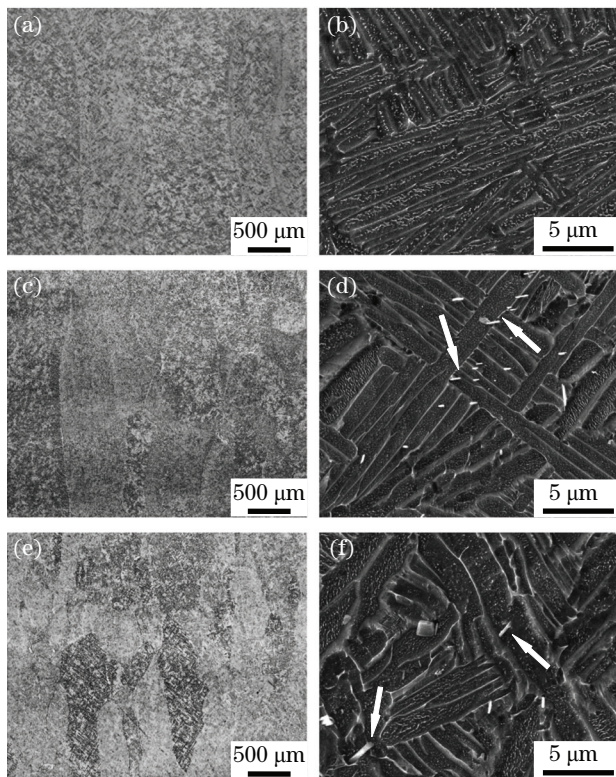


图 3 LDM 技术制备的不同 B 含量的 Ti-6Al-4V 合金的显微结构形貌, 箭头所示为 TiB 晶须。(a)(b)

Fig. 3 Morphologies of microstructures of Ti-6Al-4V alloys with different B contents prepared by LDM technology, arrows show TiB whiskers. (a)(b) 0.00% B; (c)(d) 0.05% B; (e)(f) 0.50%

合金 B 含量为 0.05% 时, 原始  $\beta$  柱状晶的直径的范围为 500~600  $\mu\text{m}$ , 如图 3(c)所示。在图 3(d)所示的 SEM 图像中, 片层状  $\alpha$  相宽度的范围为 1~1.5  $\mu\text{m}$ , 长宽比约为 16。当 B 含量继续增加时, 原始  $\beta$  柱状晶直径减小, 片层状  $\alpha$  相的宽度增加并且长宽比减小。图 3(e)中 B 的含量为 0.50%, 此时原始  $\beta$  柱状晶的直径不足 400  $\mu\text{m}$ , 片层状  $\alpha$  相的宽度约为 2  $\mu\text{m}$ , 片层状  $\alpha$  相的长宽比为 8。

图 4 为原始  $\beta$  柱状晶的直径和片层状  $\alpha$  相的长宽比随 B 含量的变化趋势。可以发现,随着 B 含量的增加,原始  $\beta$  柱状晶的直径明显减小,这表明 B 的添加可以促进  $\beta$  柱状晶的细化。晶粒细化现象背后的机理是当熔池形成时,B 与基体 Ti 元素发生反应,生成的 TiB 作为熔池凝固时的形核孕育剂,促进非匀质形核发生,导致了  $\beta$  柱状晶尺寸的减小。在增材制造过程中,第二相颗粒对  $\beta$  柱状晶细化具有明显的促进作用,稀土元素<sup>[34]</sup>、C<sup>[35]</sup> 和 Si<sup>[36]</sup> 元素都能够细化显微组织,甚至在合适的温度梯度和冷却速度条件下,实现柱晶-等轴晶转变(CET)。

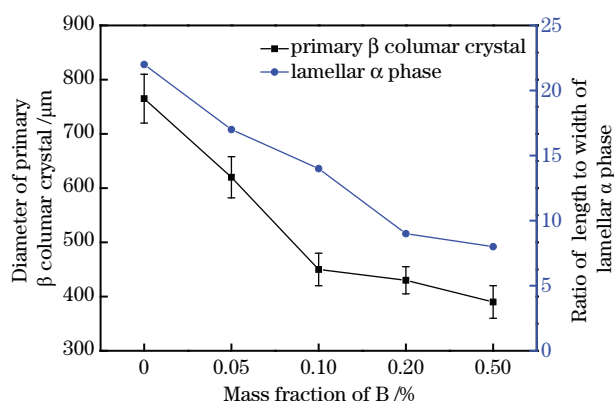


图 4 原始  $\beta$  柱状晶直径、片层状  $\alpha$  相的长宽比随 B 含量的变化趋势图

Fig. 4 The variation trend diagrams of primary  $\beta$  columnar crystal diameter and ratio of length to width of lamellar  $\alpha$  phase with B content

根据图 3 所示的结果,所有样品中的 TiB 的形貌均为直径范围为 100~200 nm 的晶须状,且均匀分布在整个显微组织中。TiB 在 B 含量为 0.10% 的样品中的明场 TEM 图像和选区电子衍射图如图 5 所示。通过样品检测发现,随着 B 含量增加,针状 TiB 的直径和长度呈增加趋势。影响 TiB 长大的主要因素为熔池温度,钛基复合材料中 TiB 的直径和长度的表达式<sup>[37-38]</sup> 分别为

$$x = \sqrt{t}, \quad (1)$$

$$k = k_0 \exp\left(\frac{-Q_K}{2RT}\right), \quad (2)$$

式中: $x$  代表直径; $k$  代表与温度相关的长大速率; $t$  代表熔池持续时间; $k_0 = 17.07 \times 10^{-4} \text{ m/s}^{1/2}$  和  $Q_K = 190.3 \text{ kJ/mol}$ <sup>[37]</sup> 分别代表 TiB 的频率因数和激活能; $R$  代表气体常量; $T$  代表熔池温度。在相同的 LDM 工艺下,B 含量的增加会增强 B 与 Ti 原子间的放热反应,进而熔池温度会得到提高。在高温状态下,熔池的保持时间会延长,故获得的针状

TiB 的直径和长度都会增大。

TiB 的晶格为  $B_{27}$  正交结构,B 原子呈锯齿状连续排列,在 [010] 方向有很强的 B—B 键,原子结构具有高度非对称性,结合强度高。在形核时,与 [100]、[101] 和 [001] 方向相比,沿 [010] 方向的生长速度更快,易生成针状或者棒状 TiB<sup>[39-41]</sup>。TiB 晶格与 Ti 基体晶格错配小,且存在  $(10\bar{1}0)\alpha/(111)\text{TiB}$  的取向关系<sup>[33-34]</sup>,故在基体  $\alpha$  相发生形变时,TiB 与基体间能够实现有效的协调效果。

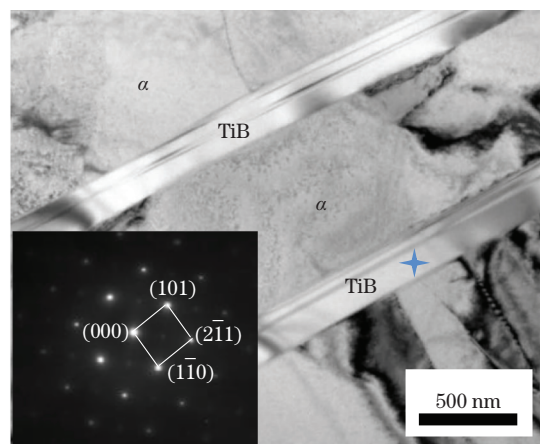


图 5 0.10% B 含量的样品中 TiB 明场 TEM 图像及其选区电子衍射图(左下角)

Fig. 5 Bright-field TEM image of TiB and selected area electron diffraction pattern (bottom left corner) in sample with B content of 0.10%

### 3.3 拉伸性能

随着 B 含量的变化,LDM 技术制造的 Ti-6Al-4V 合金的显微组织形貌和相组成均发生变化,这必然会导致材料性能的改变。LDM 技术制造的不同 B 含量 Ti-6Al-4V 合金拉伸曲线如图 6 所示。

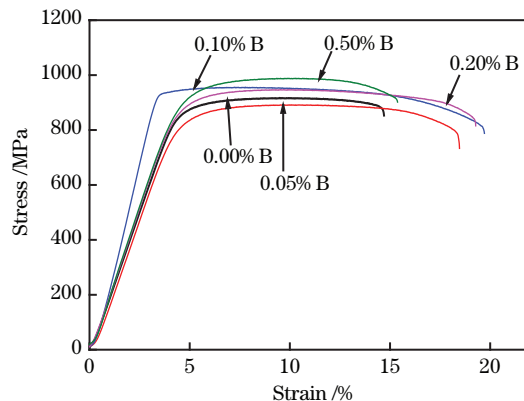


图 6 LDM 技术制备的不同 B 含量 Ti-6Al-4V 合金拉伸曲线  
Fig. 6 Tensile curves of Ti-6Al-4V alloys with different B contents prepared by LDM technology

从图 6 中可以看出,B 元素明显影响了合金的强度和塑性。B 含量为 0.00% 时,合金屈服强度为

845 MPa, 抗拉强度为 940 MPa, 延伸率不足 15%。当合金中加入 B 元素时, 强度随 B 含量的增加而增加, 同时延伸率除 B 含量为 0.50% 的合金外均达到 18% 以上。B 含量为 0.50% 的合金的屈服强度为 920 MPa, 抗拉强度为 980 MPa, 且延伸率为 15.5% 高于未添加 B 的合金。

根据 Hall-Petch 关系, 合金组织的细化可以提高合金的强度和塑性。从图 4 中可以看出, B 含量的增加有效地减小了原始  $\beta$  柱状晶的直径, 同时, 也促进了柱状晶内部片层状  $\alpha$  相长宽比的减小。TiB 使得熔池凝固所需过冷度减小<sup>[37]</sup>, 进而原始  $\beta$  柱状晶形核率增加, 柱状晶生成时刻相对提前, 柱状晶尺寸减小。凝固时刻提前、凝固温度升高, 为后续的片层状  $\alpha$  相的生成与粗化提供了更多时间。随着 B 含量的增加, 片层状  $\alpha$  相的长宽比降低, 这是因为 B 和基体 Ti 发生原位反应时释放的热量增多, 在一定程度上降低了熔池的冷却速度, 促进了片层状  $\alpha$  相的宽化。结合拉伸结果与 Hall-Petch 关系可知, 原始  $\beta$  柱状晶的细化有助于合金强度和塑性的提升, 同时, 片层状  $\alpha$  相的粗化也提高了合金的强度和塑性。

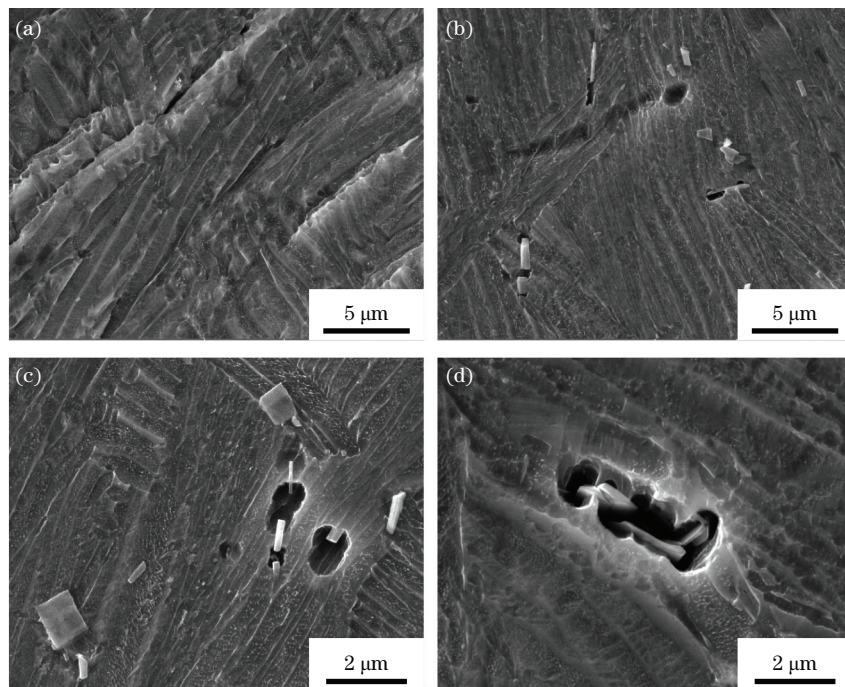


图 7 TiB 对拉伸时变形的协调作用。(a) 当不含 B 时, Ti-6Al-4V 合金中大尺寸滑移带;(b) 当 B 含量为 0.2% 时, TiB 对变形的阻碍与协调;(c) 针状 TiB 在变形中断裂并在基体上形成连续孔洞;(d) 片状 TiB 在变形中被拉断, 在基体界面上形成塑性断裂面

Fig. 7 Coordination effect of TiB on deformation during tension. (a) Large-size slip band in Ti-6Al-4V alloy without B; (b) obstruction and coordination of deformation by TiB when B content is 0.2%; (c) needle-like TiB fractures during deformation, forming continuous holes in the matrix; (d) lamellar TiB is broken during deformation, forming a plastic fracture surface on the interface of matrix

图 7 为 TiB 对拉伸时变形的协调作用。在不含 B 时,  $\beta$  柱状晶直径较大, 此时在应力作用下的片层状  $\alpha$  相的内部容易发生大尺寸的剪切滑移, 进而影响材料强度和塑性, 如图 7(a)所示。在图 7(b)中, 当有硼化物强化时, 变形被有效阻止, 片层状  $\alpha$  相内部大尺寸的剪切带不易形成。

在图 7(c)中, TiB 因受基体变形作用而发生断裂, 并在基体上形成连续分布的断裂孔洞。当基体发生塑性变形时, 针状 TiB 断裂形成的连续孔洞易连接融合为一体, 形成微裂纹。当合金中针状 TiB 过多时, 微裂纹分布密度也同时增加, 造成应力集中, 导致基体裂纹快速长大, 引起材料断裂。在图 7(d)中, 可以发现, 片状 TiB 与基体分离时, 在基体上形成微裂纹。与较长的裂纹相比, 微裂纹更容易造成基体的断裂过, 但因整体上片状 TiB 含量较低, 因此未做深入分析。故合金中过多的 TiB 在提高合金强度的同时, 降低了合金的塑性, 这验证了图 6 所示的现象。

当 B 含量为 0.10% 时, 合金具有最佳的强度塑性匹配; 当 B 含量为 0.20% 时, 塑性有所降低; 当 B 含量增至 0.50% 时, 塑性进一步降低。

## 4 结 论

首先,对激光增材制造的不同B含量的Ti-6Al-4V合金中的相组成及其可能的形成方式进行了探讨。接着,观察了显微组织特征并对各相形貌进行了统计与说明。随后,测试了合金样品的拉伸性能。最后,结合相组成与组织特征,对硼化物第二相对合金力学性能的强化机制进行了阐述。

可以发现:在LDM条件下,B在熔池中与基体Ti发生反应,原位形成针状的TiB第二相。TiB对合金具有明显的强化作用,主要体现在原始 $\beta$ 柱状晶的细化和片层状 $\alpha$ 相长宽比的降低。在B含量为0.10%时,合金的可塑性最高。在B含量为0.50%时,合金强度最高,塑性低于其他B含量的合金,但仍高于未添加B的合金。此外,合金中过多的针状TiB在基体变形时,易在基体上形成连续孔洞,且TiB过多容易造成后续基体变形时应力集中,加速裂纹扩展速度,造成合金的塑性降低。

## 参 考 文 献

- [1] Gu D D, Zhang H M, Chen H Y, et al. Laser additive manufacturing of high-performance metallic aerospace components[J]. Chinese Journal of Lasers, 2020, 47(5): 0500002.  
顾冬冬, 张红梅, 陈洪宇, 等. 航空航天高性能金属材料构件激光增材制造[J]. 中国激光, 2020, 47(5): 0500002.
- [2] Huang L J, Geng L. Strengthening and toughening mechanisms of the second phase in titanium alloys and titanium matrix composites[J]. Materials China, 2019, 3(38): 215-222.  
黄陆军, 耿林, 彭华新. 钛合金与钛基复合材料第二相强韧化[J], 中国材料进展, 2019, 3(38): 215-222.
- [3] Huo H, Liang Z Y, Zhang A F, et al. Anisotropy of mechanical properties of laser-cladding-deposited TC4 titanium alloy containing boron[J]. Chinese Journal of Lasers, 2019, 46(12): 1202008.  
霍浩, 梁朝阳, 张安峰, 等. 激光熔覆沉积含硼TC4钛合金力学性能的各向异性[J]. 中国激光, 2019, 46(12): 1202008.
- [4] Tjong S C, Mai Y W. Processing-structure-property aspects of particulate- and whisker-reinforced titanium matrix composites[J]. Composites Science and Technology, 2008, 68(3/4): 583-601.
- [5] Okulov I V, Kühn U, Marr T, et al. Deformation and fracture behavior of composite structured Ti-Nb-Al-Co(-Ni) alloys [J]. Applied Physics Letters, 2014, 104(7): 071905.
- [6] Han J H, Kim K B, Yi S, et al. Formation of a bimodal eutectic structure in Ti-Fe-Sn alloys with enhanced plasticity [J]. Applied Physics Letters, 2008, 93(14): 141901.
- [7] Yang D K, Hodgson P D, Wen C E. Simultaneously enhanced strength and ductility of titanium via multimodal grain structure [J]. Scripta Materialia, 2010, 63(9): 941-944.
- [8] Yin W H, Xu F, Ertorer O, et al. Mechanical behavior of microstructure engineered multi-length-scale titanium over a wide range of strain rates [J]. Acta Materialia, 2013, 61(10): 3781-3798.
- [9] Long Y, Wang T, Zhang H Y, et al. Enhanced ductility in a bimodal ultrafine-grained Ti-6Al-4V alloy fabricated by high energy ball milling and spark plasma sintering [J]. Materials Science and Engineering: A, 2014, 608: 82-89.
- [10] Qi Z J, Zhang X X, Wang Y Y, et al. Effect of B on microstructure and tensile properties of laser additive manufactured TC4 alloy [J]. Chinese Journal of Lasers, 2020, 47(6): 0602002.  
齐振佳, 张晓星, 王豫跃, 等. 硼对激光增材制造TC4微观组织及力学性能的影响[J]. 中国激光, 2020, 47(6): 0602002.
- [11] Zhang L C, Das J, Lu H B, et al. High strength Ti-Fe-Sn ultrafine composites with large plasticity [J]. Scripta Materialia, 2007, 57(2): 101-104.
- [12] Meng Y, Huang L J, Zhang M J, et al. Effect of boron on the microstructure and tensile properties of Ti-1023 alloy[J]. Titanium Industry Progress, 2016, 33(4): 26-30.  
孟瑶, 黄利军, 张明杰, 等. 硼对Ti-1023合金组织与性能的影响[J]. 钛工业进展, 2016, 33(4): 26-30.
- [13] Kühn U, Mattern N, Gebert A, et al. Nanostructured Zr- and Ti-based composite materials with high strength and enhanced plasticity [J]. Journal of Applied Physics, 2005, 98(5): 054307.
- [14] Zhang L C, Lu H B, Mickel C, et al. Ductile ultrafine-grained Ti-based alloys with high yield strength[J]. Applied Physics Letters, 2007, 91(5): 051906.
- [15] Huang L Q, Wang L H, Qian M, et al. High tensile-strength and ductile titanium matrix composites strengthened by TiB nanowires [J]. Scripta Materialia, 2017, 141: 133-137.
- [16] Jiao Y, Huang L J, Duan T B, et al. Controllable two-scale network architecture and enhanced mechanical properties of  $(\text{Ti}_5\text{Si}_3 + \text{TiBw})/\text{Ti}6\text{Al}4\text{V}$  composites[J]. Scientific Reports, 2016, 6: 32991.

- [17] Jiao Y, Huang L J, Wang S, et al. Effects of first-scale TiBw on secondary-scale  $Ti_5Si_3$  characteristics and mechanical properties of *in situ* ( $Ti_5Si_3 + TiBw$ )/ $Ti_6Al_4V$  composites [J]. Journal of Alloys and Compounds, 2017, 704: 269-281.
- [18] Lü Z P, Jiang S H, He J Y, et al. Second phase strengthening in advanced metal materials [J]. Acta Materialia Sinica, 2016, 10: 1183-1198.
- [19] Huang L Q, Qian M, Liu Z M, et al. *In situ* preparation of TiB nanowires for high-performance Ti metal matrix nanocomposites [J]. Journal of Alloys and Compounds, 2018, 735: 2640-2645.
- [20] Hu Y B, Zhao B, Ning F D, et al. *In-situ* ultrafine three-dimensional quasi-continuous network microstructural TiB reinforced titanium matrix composites fabrication using laser engineered net shaping [J]. Materials Letters, 2017, 195: 116-119.
- [21] Hu Y B, Cong W L, Wang X L, et al. Laser deposition-additive manufacturing of TiB-Ti composites with novel three-dimensional quasi-continuous network microstructure: effects on strengthening and toughening [J]. Composites Part B, 2018, 133: 91-100.
- [22] Sun S C, Tian Y J, Hu C, et al. Study on strengthening effect of TiBw on matrix in high temperature titanium matrix composites [J]. Titanium Industry Progress, 2020, 37(3): 15-19.  
孙世臣, 田玉晶, 胡辰, 等. TiBw 对高温钛基复合材料基体的强化作用研究 [J]. 钛工业进展, 2020, 37(3): 15-19.
- [23] Martina F, Colegrave P A, Williams S W, et al. Microstructure of interpass rolled wire + arc additive manufacturing Ti-6Al-4V components [J]. Metallurgical and Materials Transactions A, 2015, 46(12): 6103-6118.
- [24] Bermingham M J, StJohn D H, Krynen J, et al. Promoting the columnar to equiaxed transition and grain refinement of titanium alloys during additive manufacturing [J]. Acta Materialia, 2019, 168: 261-274.
- [25] de Formanoir C, Martin G, Prima F, et al. Micromechanical behavior and thermal stability of a dual-phase  $\alpha + \alpha'$  titanium alloy produced by additive manufacturing [J]. Acta Materialia, 2019, 162: 149-162.
- [26] Xia M J, Liu A H, Hou Z W, et al. Microstructure growth behavior and its evolution mechanism during laser additive manufacture of *in situ* reinforced ( $TiB + TiC$ )/Ti composite [J]. Journal of Alloys and Compounds, 2017, 728: 436-444.
- [27] Kumar P, Ramamurty U. Microstructural optimization through heat treatment for enhancing the fracture toughness and fatigue crack growth resistance of selective laser melted  $Ti_6Al_4V$  alloy [J]. Acta Materialia, 2019, 169: 45-59.
- [28] Attar H, Löber L, Funk A, et al. Mechanical behavior of porous commercially pure Ti and Ti-TiB composite materials manufactured by selective laser melting [J]. Materials Science and Engineering: A, 2015, 625: 350-356.
- [29] Wang W, Wang D, Li C F, et al. Effect of post heat treatment on microstructure and mechanical properties of Ti-6Al-4V jointing parts proceeded by laser additive manufacturing [J]. Materials Science and Engineering: A, 2020, 788: 139544.
- [30] Li X D, Li C F, Liu Y M, et al. Fracture behavior under tensile loading of Ti-6Al-4V alloy manufactured by selective laser melting processing [J]. Chinese Journal of Rare Metals, 2021, 45(3): 279-287.  
李晓丹, 李长富, 刘艳梅, 等. 选区激光熔化 Ti-6Al-4V 钛合金的拉伸断裂行为研究 [J]. 稀有金属, 2021, 45(3): 279-287.
- [31] Zhao Z, Chen J, Tan H, et al. Microstructure and mechanical properties of laser repaired TC4 titanium alloy [J]. Rare Metal Materials and Engineering, 2017, 46(7): 1792-1797.  
赵庄, 陈静, 谭华, 等. 激光修复 TC4 钛合金显微组织与力学性能 [J]. 稀有金属材料与工程, 2017, 46(7): 1792-1797.
- [32] Yang G, Wang B, Qin L Y, et al. Microstructure and properties of TC4 titanium alloy by laser deposition and wire & arc additive manufacturing [J]. Chinese Journal of Rare Metals, 2018, 42(9): 903-908.  
杨光, 王斌, 钱兰云, 等. 激光和电弧增材制造 TC4 钛合金组织和性能研究 [J]. 稀有金属, 2018, 42(9): 903-908.
- [33] Galarraga H, Warren R J, Lados D A, et al. Effects of heat treatments on microstructure and properties of Ti-6Al-4V ELI alloy fabricated by electron beam melting (EBM) [J]. Materials Science and Engineering: A, 2017, 685: 417-428.
- [34] Li W, Yang Y, Liu J, et al. Enhanced nanohardness and new insights into texture evolution and phase transformation of  $TiAl/TiB_2$  *in-situ* metal matrix composites prepared via selective laser melting [J]. Acta Materialia, 2017, 136: 90-104.
- [35] Yang C, Jiang H, Hu D, et al. Effect of boron concentration on phase transformation texture in as-solidified  $Ti_{44}Al_8Nb_xB$  [J]. Scripta Materialia, 2012, 67(1): 85-88.
- [36] Åkerfeldt P, Antti M L, Pederson R. Influence of microstructure on mechanical properties of laser

- metal wire-deposited Ti-6Al-4V [J]. Materials Science and Engineering: A, 2016, 674: 428-437.
- [37] Zhao H, Ho A, Davis A, et al. Automated image mapping and quantification of microstructure heterogeneity in additive manufactured Ti6Al4V[J]. Materials Characterization, 2019, 147: 131-145.
- [38] Panda K B, Ravi Chandran K S. Synthesis of ductile titanium-titanium boride (Ti-TiB) composites with a beta-titanium matrix: the nature of TiB formation and composite properties[J]. Metallurgical and Materials Transactions A, 2003, 34: 1371-1385.
- [39] Xu W, Lui E W, Pateras A, et al. *In situ* tailoring microstructure in additively manufactured Ti-6Al-4V for superior mechanical performance [J]. Acta Materialia, 2017, 125: 390-400.
- [40] Mereddy S, Bermingham M J, Kent D, et al. Trace carbon addition to refine microstructure and enhance properties of additive-manufactured Ti-6Al-4V [J]. Journal of Occupational Medicine, 2018, 70 (9): 1670-1676.
- [41] Mereddy S, Bermingham M J, StJohn D H, et al. Grain refinement of wire arc additively manufactured titanium by the addition of silicon [J]. Journal of Alloys and Compounds, 2017, 695: 2097-2103.

## Study on Microstructures and Properties of Additive Manufactured Ti-6Al-4V Alloy with Boron

Li Changfu<sup>1\*</sup>, Ren Haoxian<sup>1</sup>, Bu Jiaqi<sup>1</sup>, Wang Xiangming<sup>2</sup>, Yang guang<sup>1</sup>

<sup>1</sup>Key Laboratory of Fundamental Science for National Defence of Aeronautical Digital Manufacturing Process, Shenyang Aerospace University, Shenyang, Liaoning 110136, China;

<sup>2</sup>Shenyang Aircraft Design Institute, Shenyang, Liaoning 110035, China

### Abstract

**Objective** With the gradual intense provision of service requirements and service conditions, titanium (Ti) alloys have been increasingly challenged in terms of insufficient heat resistance, easy grain boundary softening, and poor wear resistance. The secondary phase strengthening is a direct and effective method for strengthening Ti alloys. The additive manufacturing (AM) technology can control the distributions and dimensions of strengthening particles at a high feasibility level. Borides (TiB<sub>2</sub>, TiB, or B<sub>4</sub>C) are usually added into the powder for AM instead of pure boron (B). An extremely high-temperature exothermic reaction occurs between pure Ti and B, which may affect the degree of dispersion and scale of the secondary phase particles, whereas limited research has been conducted. In this study, samples are prepared through laser deposition manufacturing (LDM) process with pure B added metal powder. The characteristics of the strengthening phase and its influence on microstructures and mechanical properties are evaluated.

**Methods** Ti-6Al-4V spherical powder prepares through the plasma rotating electrode processing (PREP) with particle size distribution range of 45–180 μm. The particle size of the high-purity B powder is 5–20 μm. The two kinds of powder are mixed through the mechanical mixing method at five different mass fractions of B, i.e., 0.00%, 0.05%, 0.10%, 0.20%, and 0.50%. A AM system with a 6-kW fiber laser is used to prepare the test specimens. Before the deposition, the mixed powder is dried; the substrate is ground and cleaned. The LDM process is conducted at a laser power, scan rate, and scan interval of 1.5 kW, 8 mm/s, and 2 mm, respectively, with a layer thickness of 0.5 mm. The approximate size of the deposition blocks obtained is 25 mm × 50 mm × 8 mm. Two tensile samples are obtained from each metal sample block along the horizontal direction. Scanning electron microscopy (SEM) is used to observe the secondary phase's morphology and distribution. The mechanical properties are tested on an electronic universal testing machine. Furthermore, X-ray diffraction (XRD) phase analysis (Cu K $\alpha$ , wavelength is  $1.5418 \times 10^{-10}$  m) is conducted on X-ray diffractometer, and detailed microstructure observation and phase analysis are conducted on transmission electron microscope (TEM) with a working voltage of 200 kV.

**Results and Discussions** XRD spectra of as-deposited Ti-6Al-4V with different B contents show that  $\alpha$  phase and  $\beta$  phase are the overwhelming constitutions in Fig. 2. Boride diffraction peaks are observed with low level of relative intensity level with the increase of B content. Ti alloys prepared by LDM technology usually show a certain level of texture, and variation in the relative intensity of XRD diffraction peaks indicates changes in texture strength and type. Fig. 4 shows that with the increase of B content, the diameter of the original  $\beta$  columnar crystal is reducing,

whereas the lamellar  $\alpha$  phase is becoming short and wide. In LDM process, the addition of the secondary phase particles has a significant refining effect on metallography. In some cases, the columnar equiaxed transformation (CET) can be realized. The increase of B content would introduce more heat in the melting pool as the exothermic reaction between B and Ti. Additionally, the molten pool temperature would correspondingly be increased, and the holding time at high temperature is relatively prolonged, leading to the thickening and growth of TiB whisker. The tensile curves in Fig. 7 show that the alloy has the best strength plastic matching when mass fraction of B is 0.10%. When mass fraction of B is 0.20%, the plasticity decreases slightly. However, when mass fraction of B increases to 0.50%, the plasticity further decreases, which indicates that the more the secondary phase exists, the lower the plasticity.

**Conclusions** Different contents of pure B are added to Ti-6Al-4V alloy prepared by LDM technology. The strengthening phase of the obtained alloy and its possible formation method are discussed, and the microstructure characteristics are observed. Combined with the phase and microstructure characteristics, the strengthening mechanism of the mechanical properties of borides is discussed. Under the condition of laser AM, pure B reacts with Ti in the molten pool to form *in-situ* TiB. TiB is easy to form in the high molten pool temperature zone, and its size increases with the increase of B content. TiB shows an evident strengthening effect, reflected in the refinement of the original  $\beta$  columnar crystals and the reduction of the aspect ratio of lamellar  $\alpha$  phase. The strength and plasticity of the alloy are simultaneously improved with the increase of B content. When mass fraction of B is 0.50%, the strength is the highest, and the plasticity is low but the plasticity is still higher than that of the alloy without B. When the TiB whisker deformed in the matrix, it is more likely broken, and microcracks may grow along continuous holes.

**Key words** laser technique; laser additive manufacturing; titanium alloy; *in-situ* reaction; microstructure; mechanical properties

**OCIS codes** 140.3380; 350.3390; 350.3850; 220.4000